Eur. Phys. J. D **20**, 369–374 (2002)
DOI: 10.1140/epjd/e2002-00164-5

THE EUROPEAN PHYSICAL JOURNAL D

On the mechanism of nonradiative decay of DNA bases: ab initio and TDDFT results for the excited states of 9H-adenine

A.L. Sobolewski[1] and W. Domcke[2,a]

[1] Institute of Physics, Polish Academy of Sciences, 02668 Warsaw, Poland
[2] Institute of Physical and Theoretical Chemistry, Technical University of Munich, 85747 Garching, Germany

Received 7 May 2002
Published online 13 September 2002

Abstract. Minimum-energy reaction paths and corresponding potential-energy profiles have been computed for the lowest excited states of the amino form of 9H-adenine. Complete-active- space self-consistent-field (CASSCF) and density functional theory (DFT) methods have been employed. The potential-energy function of the lowest $^1\pi\sigma^*$ state, nominally a $3s$ Rydberg state, is found to be dissociative with respect to the stretching of the NH bond length of the azine group. The $^1\pi\sigma^*$ potential-energy function intersects not only those of the $^1\pi\pi^*$ and $^1n\pi^*$ excited states, but also that of the electronic ground state. The $^1\pi\pi^*$–$^1\pi\sigma^*$ and $^1\pi\sigma^*$–S_0 intersections are converted into conical intersections when the out-of-plane motion of the active hydrogen atom is taken into account. It is argued that the predissociation of the $^1\pi\pi^*$ and $^1n\pi^*$ states by the $^1\pi\sigma^*$ state and the conical intersection of the $^1\pi\sigma^*$ state with the S_0 state provide the mechanism for the ultrafast radiationless deactivation of the excited singlet states of adenine.

PACS. 31.15.Ew Density-functional theory – 31.25.Qm Electron correlation calculations for polyatomic molecules – 31.50.Gh Surface crossings, non-adiabatic couplings

1 Introduction

The nucleic acid bases adenine, cytosine, guanine and thymine represent some of the most important building blocks of life. To understand the mutagenic and carcinogenic effects of solar UV radiation, it is essential to know the primary mechanisms of the photochemistry of the DNA bases and the nucleosides and nucleotides (for reviews of the photophysics of DNA, see, *e.g.*, Refs. [1–3]). The lowest light-absorbing $^1\pi\pi^*$ excited states of the DNA bases lie approximately 5 eV above their respective ground states. This significant energy deposited in the molecule by light absorption could initiate a variety of photoreactions. However, the quantum yields of photoproducts involving substantial rearrangements of the heteroaromatic rings are very low [2]. It seems that these reactive decay channels are efficiently quenched by very fast nonradiative decay processes back to the electronic ground state. These ultrafast nonradiative decay processes provide DNA with a high level of intrinsic photostability [1–3].

The nonradiative processes presumably are ultrafast internal conversion and photoionization (formation of solvated electrons) in aqueous solution [4]. The fluorescence quantum yields of the DNA bases were measured at room temperature in the early 1970s and found to be $<10^{-4}$ [1,2]. Triplet quantum yields are also very small [1], indicating the dominance of internal conversion in the excited-state deactivation. While it has been widely recognized that these emission properties imply S_1 lifetimes of less than 10 ps, quantitative data on the ultrafast decay processes in the DNA bases, nucleotides and nucleosides have been obtained only recently [5–11]. The transient absorption and time-resolved fluorescence measurements have revealed nonradiative decay times of the order of a few hundred femtoseconds [6,8–11]. The fluorescence decays are complex and possibly cannot be described by single exponentials [11].

In recent years it has also been demonstrated that it is possible to obtain high-resolution electronic and vibrational spectra of isolated jet-cooled DNA bases and their clusters with typical solvent molecules [12–17]. While thymine appears to exhibit only a diffuse resonance-enhanced multi-photon ionization (REMPI) spectrum and lacks fluorescence even under isolated-molecule conditions [12], the purine bases adenine and guanine posses sharp REMPI and laser-induced fluorescence (LIF) spectra, albeit only in a very narrow energy range [13–15,18]. Very recently, REMPI spectra exhibiting sharp lines have been reported also for the pyrimidine base cytosine [19]. In all DNA bases, a low-lying nonradiative threshold is observed, at which an abrupt quenching of the fluorescence occurs [13–19]. It has been suggested that $^1\pi\pi^*$–$^1n\pi^*$ coupling is responsible for the fluorescence quenching of the $^1\pi\pi^*$ state of the DNA bases, but this argument does not

[a] e-mail: wolfgang.domcke@ch.tum.de

provide a convincing explanation of the postulated ultrashort lifetime of the $^1n\pi^*$ states [14,15,20].

Up to now only relatively few calculations of the excited states of DNA bases with *ab initio* methods have been reported. The presence of several heteroatoms with lone pairs results in the existence of a number of low-lying $^1n\pi^*$ and $^1\pi\sigma^*$ states in addition to the $^1\pi\pi^*$ states, resulting in a rather complex electronic spectrum. Moreover, the DNA bases possess several tautomers of comparable energy in the electronic ground state, which is the consequence of the mobility of some of the hydrogen atoms. Calculations of the vertical excitation spectra of the bases adenine, guanine, cytosine and thymine have been reported in references [21–27]. The RPA [21,23], CIS [20,26], CASSCF [22], CASPT2 [24–27], CIPSI [28] and TDDFT methods [29] have been employed. In a few cases, excited-state geometry optimizations have been performed for the lowest $^1\pi\pi^*$ and/or $^1n\pi^*$ states [20,28–31].

It has recently been pointed out by the present authors that excited singlet states of $\pi\sigma^*$ character are likely to play a decisive role in the photochemistry of aromatic biomolecules [32–35]. It has been shown for pyrrole, indole (the chromophore of tryptophan) and phenol (the chromophore of tyrosine) that the lowest $^1\pi\sigma^*$ states, which are usually classified as 3*s* Rydberg states, exhibit potential-energy (PE) functions which are essentially repulsive with respect to the OH (phenol) or NH (pyrrole, indole) stretching coordinate. The repulsive $^1\pi\sigma^*$ PE function intersects not only the PE functions of the $^1\pi\pi^*$ states (in indole and phenol), but also that of the electronic ground state [32,34]. These symmetry-allowed intersections of $^1A'$ and $^1A''$ states are converted into conical intersections when out-of-plane modes are taken into account [33]. *Via* predissociation of the $^1\pi\pi^*$ states and a conical intersection with the ground state, the $^1\pi\sigma^*$ states can trigger the ultrafast depopulation of the optically excited $^1\pi\pi^*$ states [35].

The $^1\pi\sigma^*$ excited states of the DNA bases have hitherto essentially been ignored. Vertical excitation energies of a few low-lying $^1\pi\sigma^*$ states have been included in the tables of references [21,30], but these numbers have not further been discussed. This situation may be related to the fact that the spectroscopic detection of these states is extremely difficult. The $^1\pi\sigma^*$ states are dark in absorption and, as will be shown below, their PE surfaces are dissociative along NH or OH stretch coordinates. Presumably for this reason, $^1\pi\sigma^*$ excited states have not been mentioned in any spectroscopic paper. On the theoretical side, the valence-Rydberg mixing occurring between the $^1\pi\pi^*$ states and quasi-degenerate Rydberg states are notoriously difficult to describe (see Refs. [36,37] and references therein). Therefore these states are often artificially removed from the excitation spectrum in CASPT2 calculations [27].

In view of the findings described in references [32–34], it appears likely that $^1\pi\sigma^*$ states may also play a prominent role in the photochemistry of the DNA bases. In the present work we report the first results of an exploratory study of $^1\pi\sigma^*$ excited states and associated reaction paths for hydrogen detachment in adenine. We consider the 9H-amino tautomer of adenine, which is known to be the lowest-energy tautomer in the electronic ground state in the gas phase [18]. From the structure of the 9H tautomer it is clear that there are two potentially active centers for hydrogen detachment, the azine (NH) and the amino (NH_2) group. We consider here the lowest $^1\pi\sigma^*$ state, associated with the azine group of 9H-adenine, as well as the lowest $^1n\pi^*$ and $^1\pi\pi^*$ states.

2 Computational methods

The geometry optimizations of ground and excited states have been performed with the complete-active-space self-consistent-field (CASSCF) method. Equilibrium geometries and reaction paths of the electronic ground state and the lowest triplet state have additionally been obtained with spin-unrestricted density-functional theory (DFT) employing the B3LYP functional. The GAMESS [38] and GAUSSIAN 98 [39] program packages have been used for these calculations.

The standard 6-31G(d,p) split-valence double-zeta Gaussian basis set with polarization functions for all atoms [40] was used in the geometry optimization of the ground (S_0) and the excited valence ($^1\pi\pi^*$ and $^1n\pi^*$) states. For the Rydberg-type $^1\pi\sigma^*$ excited-state optimizations, this basis set was supplemented with a standard set of *s* and *p* diffuse Gaussian functions [40] at the nitrogen atom in position 9, and with an additional set of *s* and *p* diffuse Gaussian functions of exponent $\zeta = 0.02$, localized at the hydrogen atom of the azine (NH) group in order to provide additional flexibility for the description of the diffuse σ^* orbital.

In the CASSCF calculations of the ground and the $^1\pi\pi^*$ excited state, the active space includes the three highest π and three lowest π^* orbitals. In the CASSCF calculations of the $^1n\pi^*$ excited state, the lowest π orbital was replaced by the appropriate lone-pair orbital, while in the respective calculations for the $^1\pi\sigma^*$ excited state, the highest π^* orbital was replaced by the lowest σ^* orbital. In all CASSCF optimizations, the active space thus correlates 6 electrons in 6 orbitals.

For the construction of the reaction path for hydrogen detachment from the azine group of adenine, the coordinate-driven minimum-energy-path approach was adopted, *i.e.*, for a given value of the NH bond length all remaining coordinates were optimized. To allow for a clear distinction of $\pi\pi^*$, $n\pi^*$ and $\pi\sigma^*$ states, the molecule has been constrained to be planar in the CASSCF excited-state calculations. (Geometry optimization of the ground state yields a slightly nonplanar amino group [29]; the energy lowering with respect to the planar form is of the order of a fraction of a kcal/mol and thus negligible for the present purposes.) This symmetry constraint was relaxed in the DFT optimization of the reaction path for hydrogen detachment in the lowest triplet state and in the ground state to allow for vibronic interactions of electronic states of different orbital nature.

Since accurate CASSCF and CASPT2 calculations employing large active spaces are tedious and time-consuming in the case of densely spaced excited states, the time-dependent DFT method (TDDFT) with the B3LYP functional has been employed for the calculation of the energy profiles along the CASSCF determined reaction-path in a given electronic state. In the TDDFT calculations, the 6-31G(d,p) Gaussian basis set was supplemented with a standard set of s and p diffuse Gaussian functions [40] at all nitrogen atoms, and with an additional set of s and p diffuse Gaussian functions of exponent $\zeta = 0.02$, localized at the hydrogen atoms of the azine (NH) and amino (NH_2) groups. The TDDFT calculations have been performed with the GAUSSIAN 98 package.

3 Results and discussion

The TDDFT/B3LYP energies for the vertical excitation from the ground state (at the CASSCF equilibrium geometry) to the three lowest excited singlet states are 5.04 eV, 5.09 eV, and 5.11 eV and are assigned to the $^1n\pi^*$, $^1\pi\pi^*$ and $^1\pi\sigma^*$ states, respectively. The corresponding oscillator strengths are 0.005, 0.205, and 0.001. For comparison with previous calculations, we can refer to the CASPT2 results of reference [27] and TDDFT results of reference [29]. Only the two lowest valence states, $^1n\pi^*$ and $^1\pi\pi^*$, can be compared. The Rydberg-type $^1\pi\sigma^*$ state is not present in the TDDFT calculations of reference [29] due to the deficiency of the basis set used, which does not contain functions diffuse enough for a proper description of this transition. The $^1\pi\sigma^*$ excitation energy has not been reported in reference [27]. Our results for the lowest valence states are in excellent agreement with the TDDFT results of reference [29] (4.97 eV and 5.08 eV, respectively). The main difference with respect to the CASPT2 results of reference [27] is the position of the $^1n\pi^*$ state (6.15 eV), while the $^1\pi\pi^*$ transition energy (5.13 eV) is in good agreement with our results. The TDDFT energy of the $^1n\pi^*$ and $^1\pi\pi^*$ transitions agrees reasonably well with the lowest band near 4.9 eV in the vapor-phase absorption spectrum of adenine [41].

The TDDFT adiabatic excitation energies (T_e values) of the three lowest excited singlet states are 4.75 eV, 4.99 eV, and 5.05 eV for the $^1n\pi^*$, $^1\pi\sigma^*$, and $^1\pi\pi^*$ states, respectively. Once again, the $^1n\pi^*$ state is the lowest state, and its adiabatic energy is in acceptable agreement with the lowest line observed in the REMPI experiment at 4.40 eV and assigned as the origin of the $^1n\pi^*$ state [14].

It is worth to notice that the energy of the optimized state is the lowest among the three excited singlet states for each of the optimized excited-state geometries. To illustrate this situation, the TDDFT/B3LYP energies of the three lowest excited singlet states ($n\pi^*$, $\pi\pi^*$ and $\pi\sigma^*$) of adenine calculated at the CASSCF-optimized geometry of the respective excited state as well as at the ground state equilibrium geometry are displayed in Figure 1. These results indicate a complex pattern of intersections and therefore strong nonadiabatic interactions between the adiabatic PE surfaces of the lowest excited singlet states of adenine.

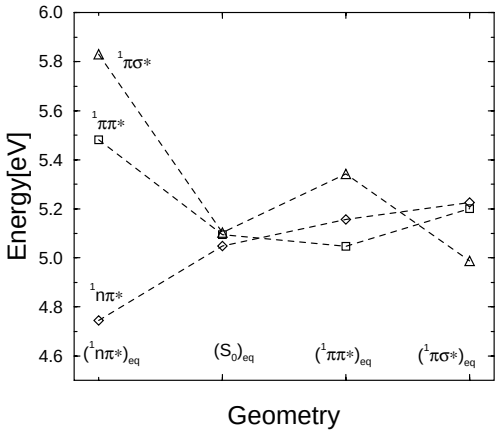

Fig. 1. Excitation energies (with respect to the ground state at its equilibrium geometry) of 9H-adenine, calculated at the equilibrium geometries of the $^1n\pi^*$, S_0, $^1\pi\pi^*$ and $^1\pi\sigma^*$ states. The $(S_0)_{eq}$ excitation energies are vertical excitation energies.

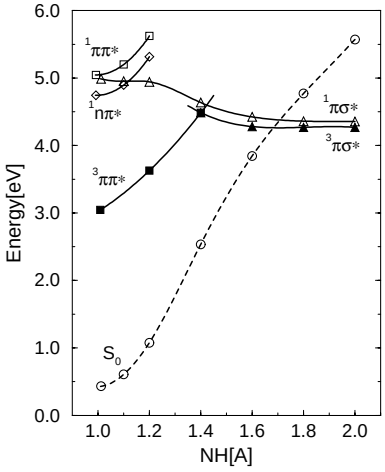

Fig. 2. Reaction-path PE profiles of 9H-adenine. The reaction coordinate is the bond length of the NH bond of the azine group. Open diamonds, squares and triangles: PE functions of the $^1n\pi^*$, $^1\pi\pi^*$ and $^1\pi\sigma^*$ states, respectively, calculated with the TDDFT method for state-specific reaction paths, optimized with the CASSCF method with planarity constraint. Circles: ground-state energy calculated at the $^1\pi\sigma^*$ optimized geometries. Full squares and triangles: PE functions of the lowest $\pi\pi^*$ and $\pi\sigma^*$ triplet states, obtained with the TDDFT method for DFT-optimized geometries.

Figure 2 shows PE profiles of the $^1n\pi^*$, $^1\pi\pi^*$ and $^1\pi\sigma^*$ states obtained as a function of the NH stretch coordinate of 9H-adenine (open symbols). The reaction paths have been optimized in the excited states at the CASSCF level, while the energy of the S_0 state is calculated at the $^1\pi\sigma^*$ optimized geometries. Although the TDDFT/B3LYP method cannot be expected to be sufficiently accurate to yield the correct ordering of the densely spaced excited states of adenine, previous calculations have indicated that the method may be reliable as far

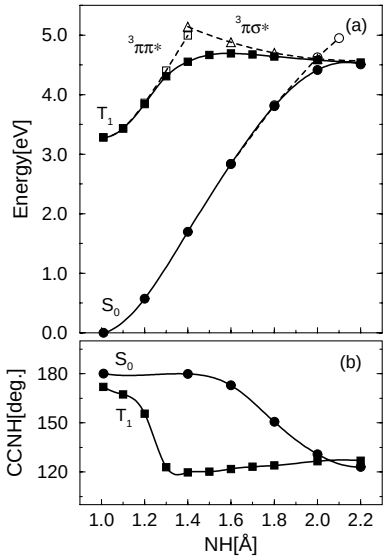

Fig. 3. (a) Reaction-path PE profiles (DFT energies) calculated at DFT-optimized geometries of S_0 and the lowest triplet states with (open symbols) and without (full symbols) planarity constraint. (b) The CCNH dihedral angle of the azine group of 9H-adenine as a function of the reaction coordinate for the S_0 (circles) and T_1 (squares) optimized reaction path.

as the shape of hydrogen-transfer PE functions is concerned [42].

The photochemical behavior of the lowest $^1\pi\sigma^*$ state of 9H-adenine is seen to be exactly the same as found previously in pyrrole [33], indole [32], and phenol [34]. At small values of the NH distance, the $^1\pi\sigma^*$ PE profile exhibits the indication of a barrier which reflects the Rydberg-to-valence transformation of the σ^* orbital. Overall, the $^1\pi\sigma^*$ PE function is repulsive and exhibits symmetry-allowed crossings with the $^1\pi\pi^*$ and S_0 states. The crossing of the $^1\pi\sigma^*$ and $^1n\pi^*$ PE functions is, in principle, an avoided one, as both states are of $^1A''$ symmetry for the planar system. The interaction of these two states appears to be weak, however. The lowest $^1n\pi^*$ state is bound like the $^1\pi\pi^*$ state with respect to hydrogen detachment.

Figure 2 shows, in addition, the PE profiles of the lowest triplet states of 9H-adenine (full symbols). These profiles were obtained with the TDDFT/B3LYP method along the DFT/B3LYP-determined reaction path. It is seen that the PEs of the $^1\pi\sigma^*$ and $^3\pi\sigma^*$ states are close to each other at these values of the NH distance, reflecting the small overlap and thus small exchange integral of the π and σ^* orbitals. A comparison of the PE functions of the $^3\pi\sigma^*$ state obtained with two different theoretical methods (TDDFT in Fig. 2 and DFT in Fig. 3) shows that they are parallel to each other, the latter being shifted upward by about 0.3 eV with respect to the former. This provides a rough estimate of the quantitative accuracy of the theoretical methods used for the description of the photophysically relevant $^1\pi\sigma^*$ state of adenine.

Figure 2 provides further support of the idea that the intersection of the $^1\pi\sigma^*$ state with the S_0 state along a suitable hydrogen-detachment coordinate is a generic phenomenon in aromatic systems containing azine or enol groups. Like in indole [32] and phenol [34], the ground state of adenine dissociates towards a $^2\sigma$ radical and the H($1s$) atom, while the lowest $\pi\sigma^*$ excited state dissociates towards the lowest dissociation limit, the $^2\pi$ ground state of the hydrogen-abstracted radical and the H($1s$) atom.

The intersections between the $^1A'$ and $^1A''$ states develop into conical intersections when out- of-plane displacements are taken into account. To investigate the nature of the intramolecular displacements active in vibronic coupling between these states, we have calculated PE profiles of the S_0 and T_1 states along the respective reaction paths at the DFT/B3LYP level without any symmetry restrictions. Such calculations can generally be performed only for the lowest state of a given multiplicity. These results are given by the full symbols in Figure 3a. It can be seen that the intersection between the $^3\pi\pi^*$ and $^3\pi\sigma^*$ states present at planar geometries develops into an avoided crossing when out-of-plane distortions are allowed and produces a barrier on the PE surface of the T_1 state. A similar effect is observed for the S_0 state and results from the vibronic interaction with the $^1\pi\sigma^*$ state at large NH distances.

To give more insight into the nature of the out-of-plane displacements involved in the coupling between the $\pi\pi^*$ and $\pi\sigma^*$ triplet states and between the $^1\pi\sigma^*$ state and the ground state, we show in Figure 3b the variation of the CCNH dihedral angle θ along the reaction paths determined for the S_0 and T_1 states respectively. In both cases the angle θ switches from planar geometry ($\theta = 180°$) at the minimum of the S_0 state or almost planar ($\theta = 171°$) at the minimum geometry of the $T_1(\pi\pi^*)$ state to the out-of-plane-distorted geometry of the $\pi\sigma^*$ state ($\theta \approx 125°$) at $R_{\mathrm{NH}} = 2.2$ Å. All other out-of-plane coordinates show only minor displacements along the reaction coordinate. It can thus be concluded that the out-of-plane motion of the detaching hydrogen atom induces the coupling of the $\pi\sigma^*$ state with both the ground state and the $\pi\pi^*$ excited state.

4 Conclusions

We have investigated in this work a particular mechanism of photoreactivity of 9H-adenine. It has been shown that the lowest $^1\pi\sigma^*$ excited state, which nominally is a $3s$ Rydberg state at the ground-state equilibrium geometry, possesses a PE function which is repulsive with respect to the stretching of the NH bond of 9H-adenine, while the low-lying $^1n\pi^*$ and $^1\pi\pi^*$ states are bound with respect to this coordinate. The PE surface of the $^1\pi\sigma^*$ state crosses not only those of the $^1n\pi^*$ and $^1\pi\pi^*$ states, but also that of the electronic ground state. These surface crossings, which are partly allowed by symmetry, develop into conical intersections when out-of-plane deformations are taken into account. The out-of-plane angle of the dissociating H atoms has been identified as the primary coupling coordinate of the conical intersections.

The qualitative topography of the PE surfaces is illustrated in Figure 4, showing the intersecting $^1\pi\pi^*$, $^1\pi\sigma^*$

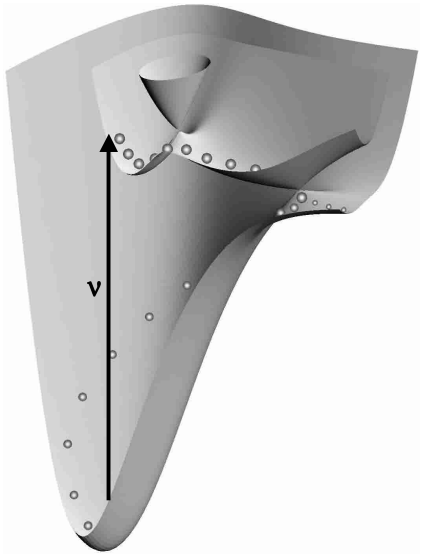

Fig. 4. Schematic view of the conically intersecting $^1\pi\pi^*$, $^1\pi\sigma^*$ and S_0 adiabatic PE surfaces and the associated photophysics. The NH-stretch coordinate is drawn to the right, the H-atom out-of-plane coordinate perpendicular to it. The arrow indicates optical excitation of the $^1\pi\pi^*$ state, the dots visualize the motion of the optically prepared wave packet.

and S_0 adiabatic PE surfaces as a function of the H-atom detachment coordinate and the H-atom out-of-plane coordinate. The arrow indicates the optical absorption process, and the dots represent schematically the motion of the optically prepared wave packet over the barrier associated with the $^1\pi\pi^*$–$^1\pi\sigma^*$ conical intersection, the bifurcation of the wave packet at the $^1\pi\pi^*$–S_0 conical intersection, and the relaxation on the electronic ground-state PE surface.

The present results are preliminary as far as the applied electronic-structure methods are concerned. More accurate excitation energies than provided by the TDDFT method are desirable, *e.g.* CASPT2 or EOM-CC excitation energies. Moreover, the photochemical reaction paths of other isomers of adenine, in particular of the 7H-amino form and of the imino forms, have to be explored, and the other three DNA bases have to be investigated with the same techniques. In view of the results obtained previously for the aromatic chromophores pyrrole, indole and phenol [32–35] it is likely, however, that the photochemical reaction mechanism discussed in the present work is generic for all four DNA bases.

Tentatively generalizing the present results, the general picture of the photochemistry of isolated DNA bases is thus as follows. As a consequence of the reduced aromaticity of these molecules owing to the presence of several heteroatoms, the light absorbing $^1\pi\pi^*$ states are located relatively high in energy. This property narrows the energy gap between the threshold of absorption (the 0–0 line of the lowest $^1\pi\pi^*$ state) and the radiationless-decay threshold. The latter is determined by the minimum of the crossing seam of the $^1\pi\pi^*$ state with the lowest $^1\pi\sigma^*$ state. The conical intersection of the $^1\pi\sigma^*$ state with the electronic ground state provides a pathway for ultrafast (femtosecond) internal conversion to the ground state, thus bypassing the potentially reactive triplet states. This qualitative picture explains the unusual LIF spectra of jet-cooled purine bases, with sharp and isomer-specific cut-offs of the fluorescence. Since the $^1n\pi^*$ states are of the same symmetry species as the $^1\pi\sigma^*$ states for planar systems, they may interact more directly with the repulsive $^1\pi\sigma^*$ states and may therefore acquire shorter lifetimes. Indications of a shorter lifetime of $^1n\pi^*$ states have been found in several experiments [14,15]. It will be interesting to see whether forthcoming calculations of the specific locations of the surface crossings of the $^1\pi\pi^*$ and $^1n\pi^*$ states with predissociative $^1\pi\sigma^*$ states can provide the explanation of the molecule-specific and isomer-specific photophysics of the jet-cooled DNA bases.

The photophysics of DNA bases in the condensed phase is a very interesting topic which is, however, beyond the scope of the present work. In recent calculations on the photochemistry of indole-water and phenol-water clusters it has been found that the Rydberg-like $^1\pi\sigma^*$ state is not destabilized, as may have been expected, but rather stabilized relative to the $^1\pi\pi^*$ states [34,43]. The origin of this unexpected phenomenon is the very large dipole moment (≈10 Debye) of the $^1\pi\sigma^*$ state [32,34]. The stabilization of the $^1\pi\sigma^*$ state relative to the $^1\pi\pi^*$ states lowers the minimum of the crossing seam in polar environments. The expected result is a complete quenching of the $^1\pi\pi^*$ fluorescence. Moreover, calculations on clusters of pyrrole, indole and phenol with water have revealed that the $^1\pi\sigma^*$ states trigger a hydrogen-transfer process from the chromophore to the aqueous environment, resulting in a radical pair (for example, the pyrrolyl radical and the hydronium radical in the case of the pyrrol-H_2O cluster) [34,43,44]. The H_3O radical has been found to decompose into a solvated H_3O^+ cation and a solvated electron cloud in larger clusters [34, 43,44]. The formation of solvated electrons has long been known to be an important channel in the photochemistry of DNA bases in aqueous solution [4,8]. It is likely that H-atom ejection driven by repulsive $^1\pi\sigma^*$ states is an essential mechanism of the photochemistry of DNA bases in protic environments.

This work has been supported by the Deutsche Forschungsgemeinschaft through SFB 377 and the Committee for Scientific Research of Poland (Grant No. 3 T09A 082 19).

References

1. M. Daniels, in *Photochemistry and Photobiology of Nucleic Acids*, edited by S.Y. Wang (Academic Press, New York, 1976), Vol. 1, p. 23
2. J. Cadet, P. Vigny, in *Bioorganic Photochemistry*, edited by H. Morrison (Wiley, New York, 1990), Vol. 1, p. 1
3. P.R. Callis, Annu. Rev. Phys. Chem. **34**, 329 (1983)
4. L.P. Candeias, S. Steenken, J. Am. Chem. Soc. **114**, 699 (1992)
5. D.N. Nikogosyan, A.A. Oraevsky, V.S. Lethokov, Z. Arbieva, E.N. Dobrov, Chem. Phys. **97**, 31 (1985)

6. D.N. Nikogosyan, D. Angelov, B. Soep, L. Lindqvist, Chem. Phys. Lett. **252**, 322 (1996)
7. T. Häupl, C. Windolph, T. Jochum, O. Brede, R. Herrmann, Chem. Phys. Lett. **280**, 520 (1997)
8. A. Reuther, H. Iglev, R. Laenen, A. Lauberau, Chem. Phys. Lett. **325**, 360 (2000)
9. J.-M. Pecourt, J. Peon, B. Kohler, J. Am. Chem. Soc. **123**, 10370 (2001)
10. J. Peon, A.H. Zewail, Chem. Phys. Lett. **348**, 255 (2001)
11. T. Gustavsson, A. Sharonov, D. Markovitsi, Chem. Phys. Lett. **351**, 195 (2002)
12. B.B. Brady, L.A. Peteanu, D.H. Levy, Chem. Phys. Lett. **147**, 538 (1988)
13. E. Nir, L.I. Grace, B. Brauer, M.S. de Vries, J. Am. Chem. Soc. **121**, 4896 (1999)
14. N.J. Kim, G. Jeong, Y.S. Kim, J. Sung, S.K. Kim, Y.D. Park, J. Chem. Phys. **113**, 10051 (2000).
15. E. Nir, K. Kleinermanns, L.I. Grace, M.S. de Vries, J. Phys. Chem. A **105**, 5106 (2001).
16. E. Nir, K. Kleinermanns, M.S. de Vries, Nature **408**, 949 (2000)
17. N.J. Kim, H. Kang, G. Jeong, Y.S. Kim, K.T. Lee, S.K. Kim, J. Phys. Chem. A **104**, 6552 (2000)
18. C. Plützer, E. Nir, M.S. de Vries, K. Kleinermanns, Phys. Chem. Chem. Phys. **3**, 5466 (2001)
19. E. Nir, M. Müller, L.I. Grace, M.S. de Vries, Chem. Phys. Lett. **355**, 59 (2002)
20. A. Broo, J. Phys. Chem. A **102**, 526 (1998)
21. H.J.A. Jensen, H. Koch, P. Jørgensen, J. Olsen, Chem. Phys. **119**, 297 (1988)
22. J.M.O. Matos, B.O. Roos, J. Am. Chem. Soc. **110**, 7664 (1988)
23. J.D. Petke, G.M. Maggiora, R.E Christoffersen, J. Am. Chem. Soc. **112**, 5452 (1990)
24. M.P. Fülscher, B.O. Roos, J. Am. Chem. Soc. **117**, 2089 (1995)
25. J. Lorentzon, M.P. Fülscher, B.O. Roos, J. Am. Chem. Soc. **117**, 9265 (1995)
26. A. Broo, A. Holmén, J. Phys. Chem. A **101**, 3589 (1997)
27. M.P. Fülscher, L. Serrano-Andres, B.O. Roos, J. Am. Chem. Soc. **119**, 6168 (1997)
28. B. Mennucci, A. Toniolo, J. Tomasi, J. Phys. Chem. **105**, 7126 (2001)
29. B. Mennucci, A. Toniolo, J. Tomasi, J. Phys. Chem. **105**, 4749 (2001)
30. M.K. Shukla, J. Leszczynski, J. Phys. Chem. A **106**, 1011 (2002)
31. L.M. Salter, G.M. Chaban, J. Phys. Chem. A **106**, 4251 (2002)
32. A.L. Sobolewski, W. Domcke, Chem. Phys. Lett. **315**, 293 (1999)
33. A.L. Sobolewski, W. Domcke, Chem. Phys. **259**, 181 (2000)
34. A.L. Sobolewski, W. Domcke, J. Phys. Chem. A **105**, 9275 (2001)
35. A.L. Sobolewski, W. Domcke, C. Dedonder-Lardeux, C. Jouvet, Phys. Chem. Chem. Phys. **4**, 1093 (2002)
36. T. Müller, M. Dallos, H. Lischka, J. Chem. Phys. **110**, 7176 (1999)
37. B.O. Roos, P.-A. Malmqvist, V. Molina, L. Serrano-Andres, M. Merchan, J. Chem. Phys. **116**, 7526 (2002)
38. M.W. Schmidt *et al.*, J. Comput. Chem. **14**, 1347 (1993)
39. M.J. Frisch *et al.*, *Gaussian 98*, Gaussian Inc., Pittsburgh, PA, 1998
40. M.S. Gordon, J.S. Binkley, J.A. Pople, W.J. Pietro, W.J. Hehre, J. Am. Chem. Soc. **104**, 2797 (1982)
41. L.B. Clark, G.G. Peshel, I.J. Tinoco, J. Phys. Chem. **69**, 3615 (1965)
42. A.L. Sobolewski, W. Domcke, Phys. Chem. Chem. Phys. **1**, 3065 (1999)
43. A.L. Sobolewski, W. Domcke, Chem. Phys. Lett. **329**, 130 (2000)
44. A.L. Sobolewski, W. Domcke, Chem. Phys. Lett. **321**, 479 (2000)